LETTER

Multi-active region AlGaN UV LEDs with transparent tunnel junctions

Applied Physics Express **16**, 082001 (2023) **LETTER**
https://doi.org/**10.35848/1882-0786/acea1b**

Multi-active region AlGaN UV LEDs with transparent tunnel junctions

Agnes Maneesha Dominic Merwin Xavier[1*], Arnob Ghosh[1], Sheikh Ifatur Rahman[1], Andrew Allerman[2], Darpan Verma[3], Roberto C. Myers[1,3], Shamsul Arafin[1], and Siddharth Rajan[1,3]

[1]*Department of Electrical and Computer Engineering, The Ohio State University, Columbus, OH 43210, United States of America*
[2]*Sandia National Laboratories, Albuquerque, NM 87185, United States of America*
[3]*Department of Materials Science and Engineering, The Ohio State University, Columbus, OH 43210, United States of America*

[*]E-mail: dominicmerwinxavier.1@osu.edu

Received June 3, 2023; revised July 19, 2023; accepted July 24, 2023; published online August 3, 2023

In this work, we demonstrate two-junction UV LEDs enabled by transparent tunnel junctions. Low voltage-drop tunnel junctions were realized in $Al_{0.3}Ga_{0.7}N$ layers through a combination of high doping and compositional grading. Capacitance and current–voltage measurements confirmed the operation of two junctions in series. The voltage drop of the two-junction LED was 2.1 times that of an equivalent single-junction LED, and the two-junction LED had higher external quantum efficiency (147%) than the single junction. © 2023 The Japan Society of Applied Physics

UV light sources are essential components in many applications including illumination, backlighting, curing, sterilization, virus elimination, air disinfection, and sensing.[1–3] UV LEDs and lasers are preferred to conventional light sources such as mercury lamps due to their low cost, low power consumption, compact size, and safety.[4,5] Aluminum gallium nitride (AlGaN) is a promising material for solid-state UV LED applications because it can be p- and n-type doped, and it has a bandgap suitable for emission over a large portion UV (~203 nm–365 nm) wavelength range.[6,7] Significant research efforts in the last few decades have led to improvement in the efficiency of UV LED's[8–12] over the past decade, but AlGaN-based UV LEDs still suffer from relatively low wall-plug efficiency and lifetime when compared to visible emitters.

A recent advancement in the design of III-nitride LEDs is the use of tunnel junction (TJ) contacts.[13–27] A tunnel junction integrated LED replaces the conventional p-GaN contact[28–32] or AlGaN/AlGaN(GaN) contact[33,34] with an inter-band tunnel junction. Tunnel junctions can improve the external quantum efficiency by eliminating the need for lower bandgap contact layers, and by improving hole injection to the p-type layer. Low lifetime remains a major challenge for UV LEDs, and it has been found that the lifetime of UV LEDs drops significantly with the operating current density (J), with some reports suggesting lifetime dependence to be $1/J^3$.[35] The need to operate at relatively low current densities to ensure high lifetime leads to higher cost ($/W) since the emitters cannot be operated at higher current and power density. Tunnel junctions can enable multi-active region designs with two or more light-emitting regions, which enables high optical power density even at low current density. Previous theoretical[36] and experimental[37–41] reports were limited to visible multi-active region LEDs, and enabled substantial increases in the external quantum efficiency, and output power density while lowering efficiency droop and I^2R losses, as well as applications such as multiple wavelength emission.[42]

There is now a significant body of work on UV LEDs using AlGaN tunnel junctions. Early efforts focused on using polarization engineering (GaN or InGaN interlayers) to reduce voltage drop and improve hole injection.[13,43–48] However, to reduce absorption losses, tunnel junction designs without low-bandgap absorbing interlayers could be preferable, especially in the case of multiple active region LEDs. Transparent homojunction tunnel junctions for AlGaN-based LEDs reported previously show higher voltage drop than the ones with interlayers, due to the larger depletion width across the tunnel junction.[49–51] Recently, it was shown that a combination of compositional grading and high doping could enable higher tunnel junction conductivity.[52] In this work, we use designs similar to the graded and doped tunnel junctions reported in Ref. 52 to demonstrate multi-active regions of AlGaN-based UV LEDs.

The one and two-junction LED structures were grown on metal–organic CVD (MOCVD)-grown n-type $Al_{0.3}Ga_{0.7}N$ template (5×10^{18} cm^{-3} Si doping) with threading dislocation density (TDD) estimated to be 2×10^9 cm^{-2}. The samples were grown using a Veeco Gen 930 N_2 plasma-assisted MBE (PAMBE) system equipped with effusion cells for metallic Ga, Mg, Si, and Al. An rf-tuned plasma power of 300 W and N_2 flow rate of 2.25 sccm was used, corresponding to a nominal growth rate of 246 nm h^{-1} (estimated from X-ray diffraction measurements of superlattice structures). The growth was carried out in the "intermediate" regime where excess Ga droplets do not accumulate.[53,54] The LED/TJ stack begins with the growth of 90 nm n-$Al_{0.3}Ga_{0.7}N$ (Si = 1×10^{19} cm^{-3}). The active region consists of three pairs of 2.5 nm $Al_{0.15}Ga_{0.85}N$ quantum wells and 7 nm $Al_{0.3}Ga_{0.7}N$ quantum barriers grown at 750 °C (T_{sub}). This was followed by an 11.5 nm p-$Al_{0.46}Ga_{0.54}N$ acting as the electron blocking layer (EBL) and a 61.5 nm p-$Al_{0.3}Ga_{0.7}N$ (Mg = 5×10^{19} cm^{-3}) grown at 720 °C. The transparent tunnel junction (TJ) was then grown using graded $p^{++} - Al_{0.5}Ga_{0.5}N \rightarrow p^{++} - Al_{0.3}Ga_{0.7}N$ (Mg = 1×10^{20} cm^{-3}) and graded $n^{++} - Al_{0.3}Ga_{0.7}N \rightarrow n^{++} - Al_{0.5}Ga_{0.5}N$ (Si = 3×10^{20} cm^{-3}) to take advantage of induced 3D polarization charges. This stack was repeated for the dual junction LED. After the completion of the LED/TJ stack, 170 nm of n-$Al_{0.3}Ga_{0.7}N$ (Si = 2×10^{19} cm^{-3}) and 25 nm of n^+- $Al_{0.3}Ga_{0.7}N$ (Si = 1×10^{20} cm^{-3}) was grown on both the samples as the top n layers. The epitaxial structures of the single and dual junction LEDs and the LED/TJ stack are shown in Figs. 1(a)–1(d)

Device fabrication began with mesa isolation using inductively-coupled plasma reactive ion etching (ICP-RIE, $BCl_3/Cl_2/Ar$), followed by deposition of ohmic metal contacts for the top and bottom n-type layers. Ti/Al/Ni/Au was deposited as the bottom contact and annealed at 850 °C for 30 s. Non-alloyed Al/Ni/Au was used as the top contact to improve extraction efficiency. Current density–voltage (J–V)

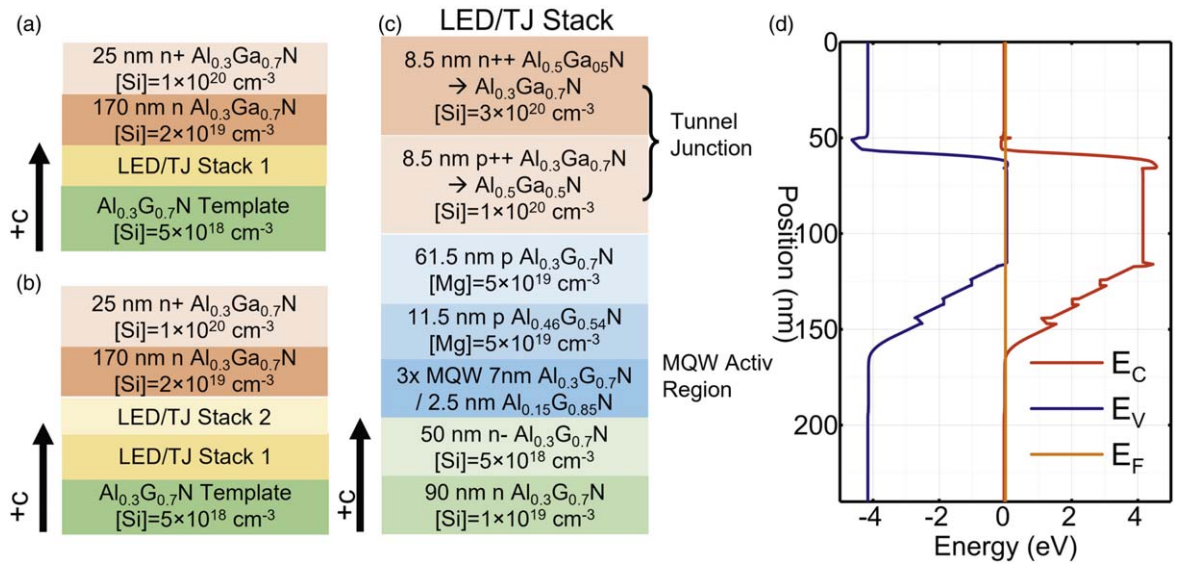

Fig. 1. The epitaxial structure of (a) the single junction LED/TJ device, (b) the dual junction (2x) LED/TJ device, and (c) the detailed epitaxial layers of the LED/TJ stack. (d) Energy band diagram corresponding to a single junction LED+TJ.

and capacitance–voltage (C–V) characteristics were measured using a Keysight B1500A semiconductor device analyzer. C–V measurements were carried out by reverse biasing the top n-contact with an excitation frequency of 5 MHz and an AC amplitude of 30 mV. The external quantum efficiency (EQE) calculations were done by measuring the optical output power from a Thorlabs PM100D optical power meter fitted with an S120VC photodiode power sensor. Electroluminescence (EL) spectra were collected from the top of the devices using a fiber optic cable coupled with a linear silicon CCD array detector-based spectrometer fitted with a cosine corrector. All the electrical and optical measurements were measured in continuous-wave operation conditions at RT.

The on-wafer electrical characteristics carried out at RT are shown in Fig. 2. Measured electrical characteristics measured on 40 μm diameter circular mesas showed that the 2-junction LED had a higher voltage than the 1-junction LED, as expected. The forward voltage drop at 20 A cm^{-2} was measured to be 6.5 V and 13.6 V for the single-junction and two-junction LEDs, respectively, corresponding to a 210% voltage scaling factor for the two-junction LED. C–V measurement [Fig. 2(c)] was performed on both samples to extract the depletion width of the LEDs, using patterns with full metal coverage. The extracted depletion width in the dual active region LED [shown in Fig. 2(d)] is 100 nm which is approximately twice the depletion width extracted from a single junction LED (52 nm) indicating two similar active regions in dual junction structure. The values are also in fairly good agreement with the effective depletion width at zero bias which was estimated to be 54 nm for the single junction and 108 nm for the double junction (from energy band diagram calculations (Bandeng[55])). The relatively flat depletion width as a function of bias also indicates high doping in the n- and p-layers on both sides of the diode active region.

The on-wafer optical power density and EQE for the two devices are shown in Figs. 3(a)–3(c). The optical power density increased from 0.88 W cm^{-2} for a single junction LED to 1.81 W cm^{-2} for a dual junction LED at 200 A cm^{-2} demonstrating a 200% increment in the power density. It has been established that the lifetime of an LED is proportional to $1/J^3$ ($\tau_{LED} \propto \frac{1}{J^3}$).[35] An output power of 0.88 W cm^{-2} requires a current density of 200 A cm^{-2}, while the same power can be achieved at 75 A cm^{-2} for a dual junction. Hence, theoretically by constructing dual junctions, the lifetime of the LED improves by a factor of 19. Figure 3(b) depicts the output power density as a function of the input power density. It is evident that although the output power density for 1x LED is slightly higher at lower input power density, it begins to droop at higher input power density. In Fig. 3(b), the dotted line shows the output and input power densities for a single junction multiplied by 2. At high input power density, it closely follows the output power density of a dual junction LED. At lower input power density, it is slightly higher and such variations can be attributed to variations in growth. The peak EQE was estimated to be 0.21% and 0.31% for the single and dual junction devices, respectively. The peak EQE scaled by 147% for the dual junction LED. The non-ideal EQE scaling may be due to degradation of the active region in the top layer due to defects introduced during the growth, or due to variations in the extraction efficiency between the two structures. Further investigation is needed to understand these effects so that the efficiency and power density of these multi-active regions can be further improved.

The on-wafer EL measurement is shown in Figs. 3(d) and 3(e). At 45 A cm^{-2}, the EL peak wavelength was 330 nm for the single junction and 335 nm for the dual junction with similar values of FWHM of 18 nms. With increasing current densities, the single and dual junction LEDs showed slight wavelength shifts from 335 nm to 330 nm and from 337 nm to 335 nm, respectively, due to the quantum confined Stark effect (QCSE). The variation in the peak wavelengths could be attributed to drift in the growth parameters between the two samples, as also reported previously for visible multi-active region LEDs.[39]

In summary, we have demonstrated fully transparent AlGaN tunnel junctions with two multi-active regions in a single device for ultraviolet LEDs accomplished by incorporating lower voltage drop tunnel junctions by a combination of high doping and polarization grading. This proof-of-concept

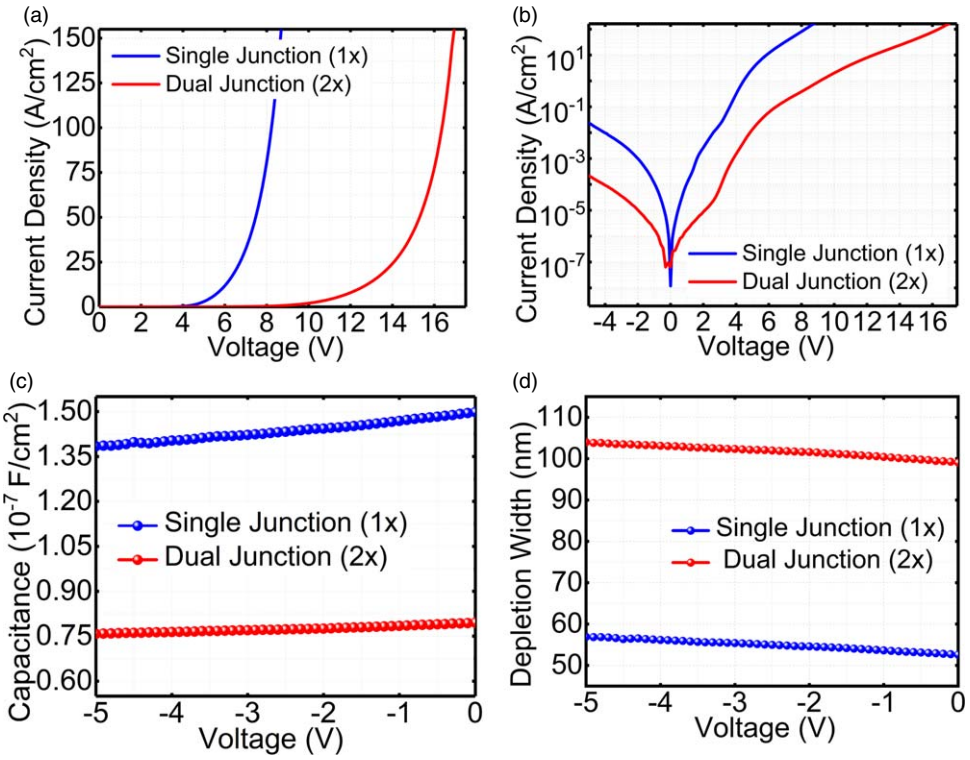

Fig. 2. Electrical characteristics in (a) linear and (b) log scale, (c) *C–V* characteristics (d) depletion width calculated from *C–V* as a function of voltage of the single and dual junction MBE grown LEDs.

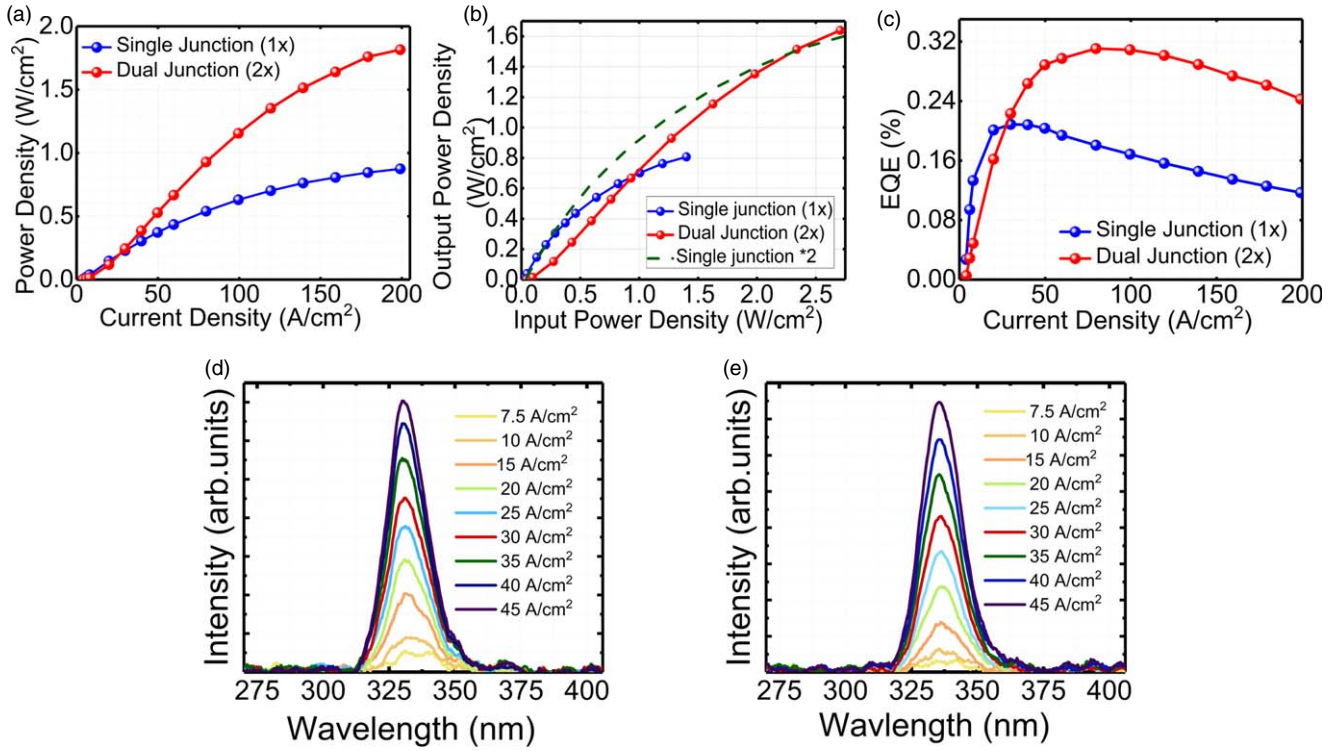

Fig. 3. On wafer (a) and (b) output power density as a function of (a) current density and (b) input power density (c) external quantum efficiencies and (d) electroluminescence spectra of the (d) single and (e) dual junction LED.

demonstration shows that the performance of UV LEDs can further be improved by well-designed active regions and by increasing the number of multi-junction active regions. This work provides a framework to enable devices with higher EQE and output power that run at low current density enabling longer lifetimes.

Acknowledgments This research was funded by the National Science Foundation (NSF) under Grant No. ECCS-2034140.

ORCID iDs Sheikh Ifatur Rahman https://orcid.org/0000-0002-9809-5102 Shamsul Arafin https://orcid.org/0000-0003-4689-2625 Siddharth Rajan https://orcid.org/0000-0003-4241-3391

1) S. L. Miller, J. Linnes, and J. Luongo, J Photochem Photobiol **89**, 777 (2013).
2) K. Song, M. Mohseni, and F. Taghipour, Water Res. **94**, 341 (2016).
3) M. Mori, A. Hamamoto, A. Takahashi, M. Nakano, N. Wakikawa, S. Tachibana, T. Ikehara, Y. Nakaya, M. Akutagawa, and Y. Kinouchi, Med. Biol. Eng. Comput. **45**, 1237 (2007).
4) M. S. Shur and R. Gaska, IEEE Trans. Electron Devices **57**, 12 (2009).
5) Y. Muramoto, M. Kimura, and S. Nouda, Semicond. Sci. Technol. **29**, 084004 (2014).
6) H. Hirayama, J. Appl. Phys. **97**, 7 (2005).
7) M. S. Shur and A. Zukauskas, *UV Solid-State Light Emitters and Detectors*, NATO Science Series II: Mathematics, Physics and Chemistry, Vol. 144, https://link.springer.com/book/10.1007/978-1-4020-2103-92004.
8) Z. Bryan, I. Bryan, J. Xie, S. Mita, Z. Sitar, and R. Collazo, Appl. Phys. Lett. **106**, 142107 (2015).
9) C. Pernot, M. Kim, S. Fukahori, T. Inazu, T. Fujita, Y. Nagasawa, A. Hirano, M. Ippommatsu, M. Iwaya, and S. Kamiyama, Appl. Phys. Express **3**, 061004 (2010).
10) K. Ban, J.-i Yamamoto, K. Takeda, K. Ide, M. Iwaya, T. Takeuchi, S. Kamiyama, I. Akasaki, and H. Amano, Appl. Phys. Express **4**, 052101 (2011).
11) A. Bhattacharyya, T. D. Moustakas, L. Zhou, D. J. Smith, and W. Hug, Appl. Phys. Lett. **94**, 181907 (2009).
12) T. Takano, T. Mino, J. Sakai, N. Noguchi, K. Tsubaki, and H. Hirayama, Appl. Phys. Express **10**, 031002 (2017).
13) Y. Zhang, S. Krishnamoorthy, J. M. Johnson, F. Akyol, A. Allerman, M. W. Moseley, A. Armstrong, J. Hwang, and S. Rajan, Appl. Phys. Lett. **106**, 141103 (2015).
14) B. P. Yonkee, E. C. Young, C. Lee, J. T. Leonard, S. P. DenBaars, J. S. Speck, and S. Nakamura, Opt. Express **24**, 7816 (2016).
15) S. Krishnamoorthy, F. Akyol, and S. Rajan, Appl. Phys. Lett. **105**, 141104 (2014).
16) M. Malinverni, D. Martin, and N. Grandjean, I Appl Phys Lett. **107**, 051107 (2015).
17) F. Akyol, S. Krishnamoorthy, Y. Zhang, J. Johnson, J. Hwang, and S. Rajan, Appl. Phys. Lett. **108**, 131103 (2016).
18) E. A. Clinton, E. Vadiee, S.-C. Shen, K. Mehta, P. D. Yoder, and W. A. Doolittle, Appl. Phys. Lett. **112**, 252103 (2018).
19) J. Simon, Z. Zhang, K. Goodman, H. Xing, T. Kosel, P. Fay, and D. Jena, Phys. Rev. Lett. **103**, 026801 (2009).
20) M. Kaga, T. Morita, Y. Kuwano, K. Yamashita, K. Yagi, M. Iwaya, T. Takeuchi, S. Kamiyama, and I. Akasaki, Jpn. J. Appl. Phys. **52**, 08JH06 (2013).
21) D. Minamikawa, M. Ino, S. Kawai, T. Takeuchi, S. Kamiyama, M. Iwaya, and I. Akasaki, Phys. Status Solidi b **252**, 1127 (2015).
22) D. Takasuka, Y. Akatsuka, M. Ino, N. Koide, T. Takeuchi, M. Iwaya, S. Kamiyama, and I. Akasaki, Appl. Phys. Express **9**, 081005 (2016).
23) Y. Akatsuka, S. Iwayama, T. Takeuchi, S. Kamiyama, M. Iwaya, and I. Akasaki, Appl. Phys. Express **12**, 025502 (2019).
24) P. Sohi, M. Mosca, Y. Chen, J.-F. Carlin, and N. Grandjean, Semicond. Sci. Technol. **34**, 015002 (2018).
25) S. Neugebauer, M. Hoffmann, H. Witte, J. Bläsing, A. Dadgar, A. Strittmatter, T. Niermann, M. Narodovitch, and M. Lehmann, Appl. Phys. Lett. **110**, 102104 (2017).
26) D. Hwang, A. J. Mughal, M. S. Wong, A. I. Alhassan, S. Nakamura, and S. P. DenBaars, Appl. Phys. Express **11**, 012102 (2017).
27) E. C. Young, B. P. Yonkee, F. Wu, S. H. Oh, S. P. DenBaars, S. Nakamura, and J. S. Speck, Appl. Phys. Express **9**, 022102 (2016).
28) Y. Liao, C. Thomidis, C.-k Kao, and T. D. Moustakas, Appl. Phys. Lett. **98**, 081110 (2011).
29) T. Wang, Y. Liu, Y. Lee, Y. Izumi, J. Ao, J. Bai, H. Li, and S. Sakai, J. Cryst. Growth **235**, 177 (2002).
30) G. Yang, F. Xie, K. Dong, P. Chen, J. Xue, T. Zhi, T. Tao, B. Liu, Z. Xie, and X. Xiu, Physica E Low Dimens Syst Nanostruct. **62**, 55 (2014).
31) J. Yan, J. Wang, P. Cong, L. Sun, N. Liu, Z. Liu, C. Zhao, and J. Li, Phys. Status Solidi C **8**, 461 (2011).
32) B. K. SaifAddin, A. S. Almogbel, C. J. Zollner, F. Wu, B. Bonef, M. Iza, S. Nakamura, S. P. DenBaars, and J. S. Speck, ACS Photonics **7**, 554 (2020).
33) J.-Y. Duboz, Semicond. Sci. Technol. **29**, 035017 (2014).
34) T.-Y. Wang, W.-C. Lai, S.-Y. Sie, S.-P. Chang, C.-H. Kuo, and J.-K. Sheu, Processes **9**, 1727 (2021).
35) J. Ruschel, J. Glaab, B. Beidoun, N. L. Ploch, J. Rass, T. Kolbe, A. Knauer, M. Weyers, S. Einfeldt, and M. Kneissl, Photonics Res **7**, B36 (2019).
36) F. Akyol, S. Krishnamoorthy, and S. Rajan, Appl. Phys. Lett. **103**, 081107 (2013).
37) Z. Jamal-Eddine, S. M. Hasan, B. Gunning, H. Chandrasekar, M. Crawford, A. Armstrong, S. Arafin, and S. Rajan, Appl. Phys. Lett. **117**, 051103 (2020).
38) F. Akyol, S. Krishnamoorthy, Y. Zhang, and S. Rajan, Appl. Phys. Express **8**, 082103 (2015).
39) Z. Jamal-Eddine, B. P. Gunning, A. A. Armstrong, and S. Rajan, Appl. Phys. Express **14**, 092003 (2021).
40) C. Chen, S.-J. Chang, Y.-K. Su, J.-K. Sheu, J.-F. Chen, C.-H. Kuo, and Y.-C. Lin, IEEE Photonics Technol. Lett. **14**, 908 (2002).
41) S.-J. Chang, W.-H. Lin, and W.-S. Chen, IEEE J. Quantum Electron. **51**, 1 (2015).
42) I. Ozden, E. Makarona, A. Nurmikko, T. Takeuchi, and M. Krames, Appl. Phys. Lett. **79**, 2532 (2001).
43) Y. Zhang, S. Krishnamoorthy, F. Akyol, A. A. Allerman, M. W. Moseley, A. M. Armstrong, and S. Rajan, Appl. Phys. Lett. **109**, 121102 (2016).
44) Y. Zhang, Z. Jamal-Eddine, F. Akyol, S. Bajaj, J. M. Johnson, G. Calderon, A. A. Allerman, M. W. Moseley, A. M. Armstrong, and J. Hwang, Appl. Phys. Lett. **112**, 071107 (2018).
45) Y. Zhang, S. Krishnamoorthy, F. Akyol, S. Bajaj, A. A. Allerman, M. W. Moseley, A. M. Armstrong, and S. Rajan, Appl. Phys. Lett. **110**, 201102 (2017).
46) Y. Zhang, S. Krishnamoorthy, F. Akyol, J. M. Johnson, A. A. Allerman, M. W. Moseley, A. M. Armstrong, J. Hwang, and S. Rajan, Appl. Phys. Lett. **111**, 051104 (2017).
47) A. Pandey, J. Gim, R. Hovden, and Z. Mi, Appl. Phys. Lett. **117**, 241101 (2020).
48) A. Pandey, W. J. Shin, J. Gim, R. Hovden, and Z. Mi, Photonics Res. **8**, 331 (2020).
49) K. Nagata, H. Makino, H. Miwa, S. Matsui, S. Boyama, Y. Saito, M. Kushimoto, Y. Honda, T. Takeuchi, and H. Amano, Appl. Phys. Express **14**, 084001 (2021).
50) C. Kuhn, L. Sulmoni, M. Guttmann, J. Glaab, N. Susilo, T. Wernicke, M. Weyers, and M. Kneissl, Photonics Res. **7**, B7 (2019).
51) K. Nagata, S. Anada, H. Miwa, S. Matsui, S. Boyama, Y. Saito, M. Kushimoto, Y. Honda, T. Takeuchi, and H. Amano, Appl. Phys. Express **15**, 044003 (2022).
52) A. M. Dominic Merwin Xavier, A. Ghosh, S. I. Rahman, A. Allerman, S. Arafin, and S. Rajan, Appl. Phys. Lett. **122**, 081108 (2023).
53) B. Heying, R. Averbeck, L. Chen, E. Haus, H. Riechert, and J. Speck, J. Appl. Phys. **88**, 1855 (2000).
54) B. Heying, I. Smorchkova, C. Poblenz, C. Elsass, P. Fini, S. Den Baars, U. Mishra, and J. Speck, Appl. Phys. Lett. **77**, 2885 (2000).
55) M. Grundmann, (http://my.ece.ucsb.edu/mgrundmann/bandeng/).